http://dx.doi.org/10.5012/bkcs.2012.33.4.1204

Nanocrystalline Antimony Oxide Films for Dye-Sensitized Solar Cell Applications

Ji-Hye Kim, Jiyeon Jang, Sung-Chul Kim, Chi-Hwan Han,† and Seung-Joo Kim*

Department of Chemistry, Division of Energy Systems Research, Ajou University, Suwon 443-749, Korea
**E-mail: sjookim@ajou.ac.kr*
†*Korea Institute of Energy Research, Daejeon 305-343, Korea*
Received October 28, 2011, Accepted January 4, 2012

A new photoelectrode composed of Sb_6O_{13} nanoparticles with the size of 20-30 nm has been prepared *via* thermolysis of a colloidal antimony pentoxide tetrahydrate ($Sb_2O_5{\cdot}4H_2O$) suspension. The Sb_6O_{13} electrode showed good semiconducting properties applicable to dye-sensitized solar cells (DSSCs); the energy band gap was estimated to be 3.05 ± 0.5 eV and the position of conduction band edge was close to those of TiO_2 and ZnO. The DSSC assembled with the Sb_6O_{13} photoelectrode and a conventional ruthenium-dye (*N*719) exhibited the overall photo-current conversion efficiency of 0.74% (V_{oc} = 0.76 V, J_{sc} = 1.99 mAcm^{-2}, fill factor = 0.49) under AM 1.5, 100 mWcm^{-2} illumination.

Key Words : Dye-sensitized solar cells, Antimony oxide, Sb_6O_{13}, Photoelectrode

Introduction

Dye-sensitized solar cells (DSSCs) have been attracting extensive interests owing to its high light-to-electrical energy conversion efficiency, simple fabrication process and low production cost.[1] The DSSCs are based on the dye sensitization of wide band gap semiconductors used in the form of porous nanocrystalline films. Energy conversion is achieved by injection of electrons from the photoexcited state of the sensitizer dye into the conduction band of the semiconductor. Thus the semiconductor electrode should have an appropriate band structure matching with sensitizer, large surface area and long-term stability. Many researches have been carried out to explore effective electrode materials for the application in DSSCs so far, based on simple binary oxides such as TiO_2,[1-5] ZnO,[6-9] SnO_2,[10,11] Fe_2O_3,[12] Nb_2O_5,[13,14] and CdO.[15] Recently such an effort has been extended to the more complex compounds including $SrTiO_3$[13] and Zn_2SnO_4.[16] Here we investigate the possibility of using antimony oxide as a new electrode material for DSSC. To the best of our knowledge, fabrication and photovoltaic property of antimony oxides-based DSSC have not been reported yet.

Antimony oxide system shows diversity in composition and structure due to the coexistence of both Sb^{3+} and Sb^{5+} ions in the oxides with different stoichiometries and the inclusion of water molecules into the lattice forming hydrated oxides. Pentavalent Sb^{5+} ion can be stabilized most commonly in the hydrated form, $Sb_2O_5{\cdot}nH_2O$ (n ~ 4). According to previous literatures,[17,18] on heating $Sb_2O_5{\cdot}4H_2O$ to 900 °C under ambient atmosphere, it is decomposed to Sb_2O_4 *via* complex processes including dehydration and reduction. The intermediates observed in the thermolysis process for $Sb_2O_5{\cdot}4H_2O$ are $Sb_2O_5{\cdot}2H_2O$, $Sb_2O_{5-\delta}{\cdot}xH_2O$ ($0 < x < 2$) and Sb_6O_{13}. In this study, we prepare porous Sb_6O_{13} films through thermal decomposition of $Sb_2O_5{\cdot}4H_2O$ deposited onto conducting glass and describe their photoelectrochemical properties.

Experimental

Preparation of Hydrated Antimony Pentoxide Nanoparticles. The procedures for the synthesis of $Sb_2O_5{\cdot}4H_2O$ nanoparticles were described in the literature elsewhere.[19] Typically, 10 g of antimony trioxide (Aldrich, particle size < 250 nm) and 1.0 g of poly(vinyl alcohol) were poured in 50 mL of deionized water, and then 10 mL of 30% hydrogen peroxide solution was added dropwise to the mixture with stirring. The mixture was heated up to 90 °C and maintained for 3 h. In the heating step, the mixture became a transparent pale yellow solution for a while and finally turned into a white colloidal suspension. After freeze-drying the suspension, hydrated antimony pentoxide ($Sb_2O_5{\cdot}4H_2O$) powders were obtained.

Solar Cell Assembly. An aqueous slurry was prepared by mixing 0.3 g of $Sb_2O_5{\cdot}4H_2O$, 5 mL of H_2O and 0.5 mL Triton X-100 (Aldrich). The pastes were deposited onto F-doped SnO_2 (FTO) glass supports (8 Ω/sq, Dyesol Ltd.) using a spin coater and subsequently heated for 1 h at temperature range of 450-600 °C under air. The thickness of the resultant film was measured with a surface profiler (Tencor, P-10). Dye adsorption was carried out by immersing the antimony oxide electrodes in a 0.3 mM ethanolic solution of the conventional ruthenium dye, *cis-bis* (isothiocyanato)bis-(2,20-bipyridyl-4,40-dicar-boxylato)-ruthenium(II)bis-tetrabutylammonium (*N*719, Solaronix), for 24 h at room temperature. Pt counter electrodes were prepared by spreading a drop of 5 mM hydrogen hexachloroplatinate(IV) hydrate solution on FTO glass and heating it at 550 °C for 1 h. The Pt electrode was placed over the dye-coated electrode, and the edges of the cell were sealed with thermoplastic polymer films of 65 μm thick. Sealing was finished

by pressing the two electrodes at a temperature of 130 °C for 8 min. The space between two electrodes was filled with electrolyte (0.1 M of LiI, 0.05 M of I_2, 0.6 M of 1-butyl-3-methylimidazolium iodide and 0.5M of *t*-butylpridine in 3-methoxy propionitrile).

Characterization. The powder product was characterized by transmission electron microscope (TEM) measurements (Tecnai G2 F30 S-Twin). The film morphology was investigated by a field-emission scanning electron microscope (FE-SEM) (JEOL, JSM-6700F). X-ray diffraction (XRD) data were collected using an X-ray diffractometer (Rigaku, DMAX-2200PC) with Cu K_α radiation. The flat band potential was investigated by voltammetry using a potentiostat (Pine, AFCBP1).[20] In the voltammetry process, a nanoparticles-coated FTO glass was used as the working electrode. A Pt wire and a Ag/AgCl electrode were used as the counter and reference electrodes, respectively. 0.1 M KCl aqueous solution was used as the supporting electrolyte (pH = 6.5). UV-vis diffuse reflectance data were collected in the range of 200-800 nm with a double beam Shimadzu UV-2400PC at room temperature. The data were transformed into absorbance with the Kubelka-Munk function.[21] The photoelectrochemical properties of the prepared dye-sensitized solar cell were measured by using a computer-controlled digital source meter (EG & G, Potentiostat/Galvanostat Model 273A) and a solar simulator (AM 1.5, 100 $mWcm^{-2}$, Oriel) as a light source. To estimate the dye adsorbed amount on the oxide films, the sensitized electrode was separately immersed into a 0.1 M NaOH solution in a mixed solvent (water:ethanol = 1:1), which resulted in the desorption of *N*719. The absorbance of the resulting solution was measured by a UV-vis spectrophotometer.

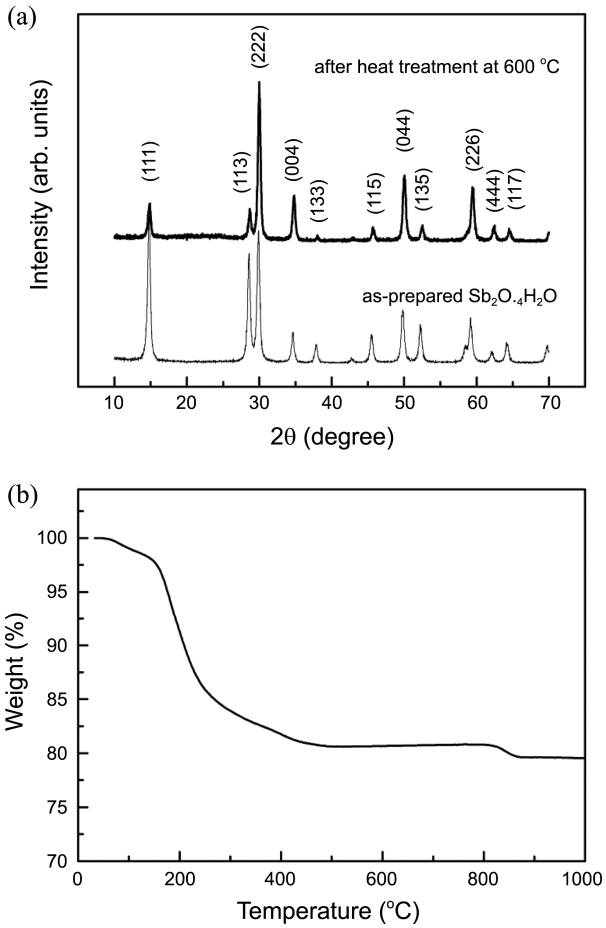

Figure 1. (a) XRD patterns of $Sb_2O_5{\cdot}4H_2O$ as prepared (bottom) and after heat treatment at 600 °C (upper). (b) TG curve of the $Sb_2O_5{\cdot}4H_2O$ precursor at heating rate of 5 °Cmin^{-1}.

Results and Discussion

The XRD patterns of Figure 1(a) reveal that the colloidal precursor obtained from oxidizing Sb_2O_3 in H_2O_2 aqueous solution was $Sb_2O_5{\cdot}4H_2O$ (JCPDS # 33-0111) and it converted to Sb_6O_{13} phase (JCPDS # 21-0804) after heat treatment at 600 °C. Both structures of $Sb_2O_5{\cdot}4H_2O$ and Sb_6O_{13} belong to a cubic pyrochlore–type with space group $Fd\bar{3}\,m$. Generally, pyrochlore structure, which has the form $A_2B_2X_6X'$, can be interpreted by two interpenetrated networks, one of BX_6 corner-sharing octahedra and another of A_2X' arranged as an anti-cristobalite sublattice.[22] In the structure of $Sb_2O_5{\cdot}4H_2O$, H^+ and $(H_2O)H^+$ ions are statistically distributed over the A sites, while Sb^{5+}, O^{2-} ions and H_2O molecules fully occupy the B, X and X sites, respectively.[18] On the other hand, Sb_6O_{13} has a defect pyrochlore structure in which the A and X' sites are partially occupied with site occupation factors of 0.5, by Sb^{3+} and O^{2-} ions, respectively. Thus Sb_6O_{13} can be represented as a structural formula of $Sb^{3+}Sb^{5+}{}_2O_6O'_{0.5}$. In order to confirm the thermal behavior of $Sb_2O_5{\cdot}4H_2O$ precursor, thermogravimetric analysis was carried out. As shown in Figure 1(b), the sample underwent stepwise decomposition. The weight loss below the temperature of 150 °C is due to the adsorbed water in precursor powder. The second weight loss, which occurred in the temperature range of 150-450 °C is associated with the liberation of water and oxygen molecules from $Sb_2O_5{\cdot}4H_2O$ lattices and also with the decomposition and the combustion of organic surfactant. Sb_6O_{13} phase started to form above 450 °C and showed a good thermal stability up to 820 °C. Additional weight loss, which occurred in the temperature range of 820-860 °C, is ascribed to the further reduction of Sb_6O_{13} to Sb_2O_4. Figure 2(a) shows the TEM image of Sb_6O_{13} powder obtained *via* heating of the $Sb_2O_5{\cdot}4H_2O$ precursor at 600 °C. Sb_6O_{13} nanoparticles show nearly spherical shape and their diameters are in the range of 20-30 nm. The selected-area electron diffraction pattern in the inset of Figure 2(a) supports the polycrystalline nature in Sb_6O_{13}. SEM image in Figure 2(b) shows the surface morphology of Sb_6O_{13} thin film deposited on FTO substrates, indicating a highly porous structure capable to provide large surface area for DSSC application.

The optical absorption spectrum of Sb_6O_{13}, which was obtained from the diffuse reflectance spectrum by using the Kubelka-Munk method,[21] is shown in Figure 3(a). The spectra of TiO_2 and ZnO, the most common electrode materials for DSSCs, are also presented for comparison. Band gaps were determined by the following dependence:[23]

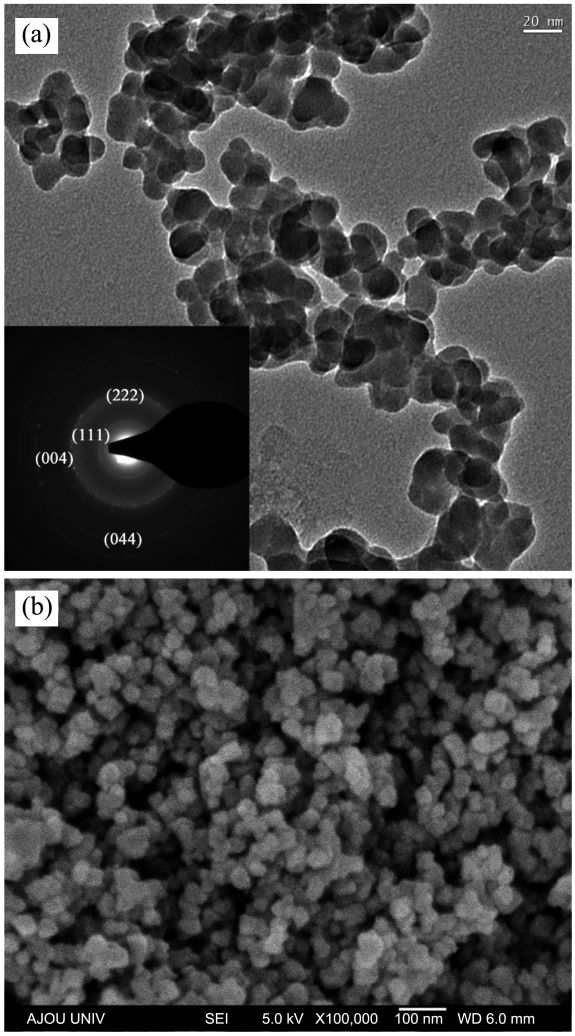

Figure 2. (a) TEM image of Sb_6O_{13} nanoparticles. The inset is electron diffraction pattern. (b) SEM image of Sb_6O_{13} nanoparticles deposited on FTO substrate.

$$(F(\mathrm{R})E)^{1/\eta} = K(E - E_g)$$

Here $F(\mathrm{R})$, K, E, and E_g are Kubelka-Munk function, proportionality constant, incident photon energy, and band gap, respectively. In the equation, η decides the characteristics of the transition in a semiconductor ($\eta = 1/2$ for direct transition; $\eta = 2$ for indirect transition).[24] Assuming that TiO_2 and Sb_6O_{13} are of indirect gaps and ZnO is of direct gap,[25,26] the E_g's are determined to be 3.25 ± 0.05 eV for TiO_2, 3.05 ± 0.5 eV for Sb_6O_{13} and 3.30 ± 0.05 eV for ZnO. In order to estimate the relative positions of conduction band, voltammogram of Sb_6O_{13} is compared with those of references such as TiO_2 and ZnO. The TiO_2 and ZnO thin film electrodes were prepared by heat treatment of appropriate precursors at 600 °C. Figure 3(b) shows the current-voltage characteristics for the thin film electrodes at pH 6.5. The steady-state cathodic current was increased with applying cathodic potential and the onset potential can be treated as a measure of the flat band potential of the semiconductor. For TiO_2 electrode, the cathodic current

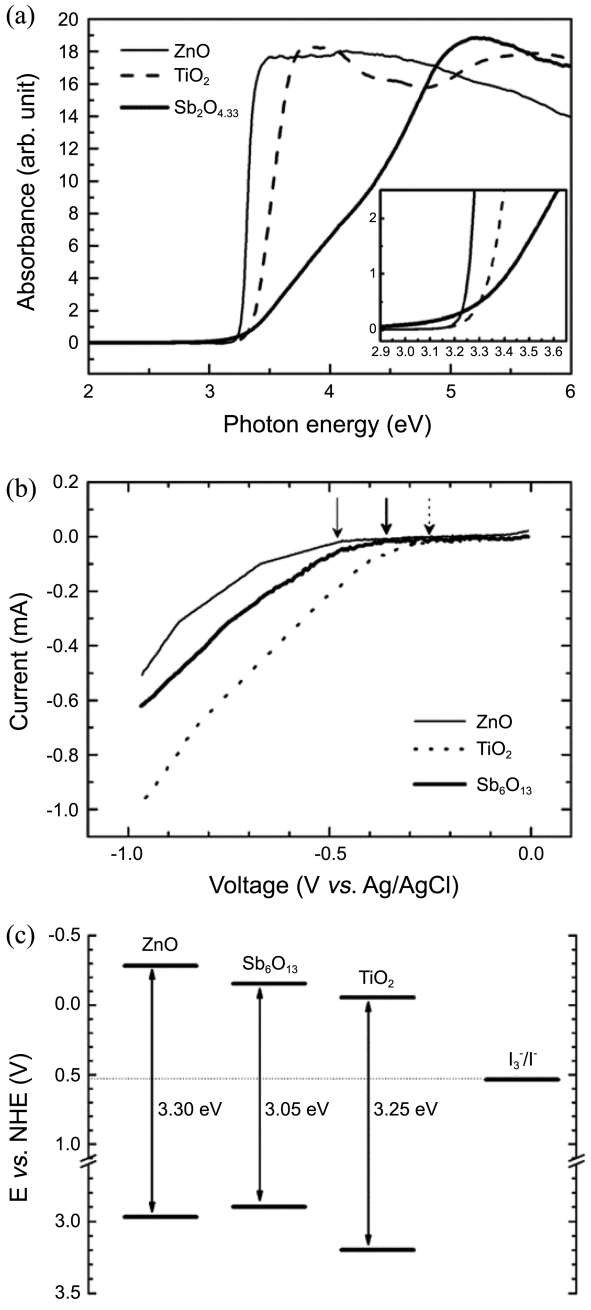

Figure 3. (a) UV-vis diffuse reflectance spectra for ZnO, TiO_2 and Sb_6O_{13}. (b) Voltammograms of ZnO, TiO_2, and Sb_6O_{13} electrodes in 0.1M KCl aqueous solution at pH = 6.5. The arrows indicate the on-set potentials for each electrode. (c) Energy-level diagram showing the relative CB positions of ZnO, TiO_2 and Sb_6O_{13} with the energy positions of I_3^-/I^-.

starts to flow at −0.25 V *versus* Ag/AgCl, whereas the current starts to flow at a lower potential (−0.48 V *versus* Ag/AgCl) for ZnO electrode. The flat band potentials for TiO_2 and ZnO electrodes are well consistent with those observed in literature.[20] The onset potential of Sb_6O_{13} was found around in −0.36 V which is between those of TiO_2 and ZnO. Such aspect indicates that the conduction band edge potential of Sb_6O_{13} is more negative toward the vacuum level than that of ZnO but less negative than TiO_2. From the energy band

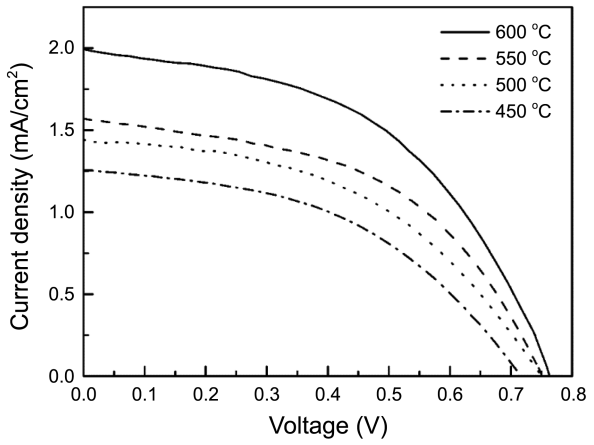

Figure 4. Photocurrent–voltage curves of DSSCs assembled with Sb_6O_{13} films calcined at various temperatures. For all the cells, the Sb_6O_{13} layer has an effective area of 0.25 cm^2 and thickness of 1.0 ± 0.1 μm. Illumination intensity is AM 1.5, 100 $mWcm^{-2}$.

gaps and the band potentials determined here, the energy band diagram of Sb_6O_{13} is schematically represented as Figure 3(c).

The *J-V* measurements of DSSCs with Sb_6O_{13} thin film photoelectrodes prepared under different temperatures were carried out. For the fabrication of the DSSCs, *N*719 dye was adsorbed on the Sb_6O_{13} thin films with the thickness of 1.0 ± 0.1 μm. The photoelectrodes were assembled with platinized FTO glass counter electrodes and liquid electrolyte. In Figure 4, an enhancement in photovoltaic performance is obviously detected for the electrode prepared at higher temperature: Under illumination (AM 1.5, 100 mW cm^{-2}), the Sb_6O_{13} photoelectrode prepared at 600 °C gives a V_{oc} of 0.76 V, a J_{sc} of 1.99 $mAcm^{-2}$, a fill factor of 49%, and an efficiency of 0.74%. The increase in J_{sc} along the preparation temperature may be due to a formation of better electric contact between nanoparticles at higher temperature. The V_{oc} values of Sb_6O_{13}-based DSSCs are comparable to typical V_{oc} values observed in TiO_2 or ZnO-based DSSCs, which is in agreement with the position of Sb_6O_{13} conduction band edge located in-between those of TiO_2 and ZnO. The lower efficiency for the Sb_6O_{13}-based DSSC compared to TiO_2 or ZnO-based ones may be attributed to the low light-harvesting capability due to insufficient dye adsorption. The amount of dye loaded on the Sb_6O_{13} electrode (~6×10^9 mol cm^2), estimated from the dye-desorption experiment, was about one-tenth of the reported values for typical TiO_2 or ZnO-based DSSCs.[1-9] The attempt to enhance the efficiency by increasing the thickness of Sb_6O_{13} was not successful, implying that the electron mobility in Sb_6O_{13} electrode is very low. The relatively poor transport ability of Sb_6O_{13} may be resulted from low density of state, indicated by the less stiff slope of absorption edge on the UV spectrum.

Conclusion

We have synthesized the nanocrystalline Sb_6O_{13} films using $Sb_2O_5{\cdot}4H_2O$ colloidal precursor. The Sb_6O_{13} phase were formed when the $Sb_2O_5{\cdot}4H_2O$ precursor was heated above 450 °C. A higher calcination temperature resulted in the higher V_{oc} and J_{sc} of the Sb_6O_{13} cell. Although the overall efficiency is still low, the high V_{oc} reaching 0.8 V observed in the ruthenium dye (*N*7190) sensitized Sb_6O_{13} cell shows a possibility of using the antimony oxide as a photoelectrode material for DSSCs. Further studies on alternative dyes and surface modification of the Sb_6O_{13} electrode may lead to improved photovoltaic performance.

Acknowledgments. This work was supported by National Research Foundation of Korea (No. 2011-0030745 and No. 2011K000581). The authors thank for Prof. N.-G. Park (Sungkyunkwan University) and Dr. T.-G. Kim (Samsung Advanced Institute of Technology) for taking part in discussions. One of the authors, S.-J. Kim is grateful to Ajou University for granting his sabbatical leave during the academic year 2010.

References

1. O'Regan, B.; Grätzel, M. *Nature* **1991**, *353*, 737.
2. Nazeeruddin, M. K.; Kay, A.; Rodicio, I.; Humphry-Baker, R.; Muller, E.; Liska, P.; Vlachopoulos, N.; Grätzel, M. *J. Am. Chem. Soc*. **1993**, *115*, 6382.
3. Thavasi, V.; Renugopalakrishnan, V.; Jose, R.; Ramakrishna, S. *Mater. Sci. Eng. R* **2009**, *63*, 81.
4. Park, N.-G.; van de Lagemaat, J.; Frank, A. J. *J. Phys. Chem. B* **2000**, *104*, 8989.
5. Kim, Y. J.; Lee, M. H.; Kim, H. J.; Lim, G.; Choi, Y. S.; Park, N.-G.; Kim, K.; Lee, W. I. *Adv. Mater*. **2009**, *21*, 3668.
6. Keis, K.; Lindgren, J.; Lindquist, S. E.; Hagfeldt, A. *Langmuir* **2000**, *16*, 4688.
7. Bauer, C.; Boschloo, G.; Mukhtar, E.; Hagfeldt, A. *J. Phys. Chem. B* **2001**, *105*, 5585.
8. Keis, K.; Magnusson, E.; Lindström, H.; Lindquist, S. E.; Hagfeldt, A. *Sol. Energy. Mater. Sol. Cells* **2002**, *73*, 51.
9. Shin, Y.-J.; Kim, K. S.; Park, N.-G.; Ryu, K. S.; Chang, S. H. *Bull. Korean Chem. Soc*. **2005**, *26*(12), 1929.
10. Bedja, I.; Hotchandani, S.; Kamat, P. V. *J. Phys. Chem*. **1994**, *98*, 4133.
11. Chappel, S.; Zaban, A. *Sol. Energy. Mater. Sol. Cells* **2002**, *71*, 141.
12. Bjoerksten, U.; Moser, U.; Grätzel, M. *Chem. Mater*. **1994**, *6*, 858.
13. Lenzmann, F.; Krueger, J.; Burnside, S.; Brooks, K.; Grätzel, M.; Gal, D.; Ruhle, S.; Cahen, D. *J. Phys. Chem. B* **2001**, *105*, 6347.
14. Sayama, K.; Sugihara, H.; Arakawa, H. *Chem. Mater*. **1998**, *10*, 3825.
15. Mane, R. S.; Pathan, H. M.; Lokhande, C. D.; Han, S.-H. *Solar. Energy* **2006**, *80*, 185.
16. Tan, B.; Toman, E.; Li, Y.; Wu, Y. *J. Am. Chem. Soc*. **2007**, *129*, 4162.
17. Golunski, S. E.; Jackson, D. *Appl. Catal*. **1989**, *48*, 123.
18. Klestchov, D.; Burmistrov, V.; Sheinkman, A.; Pletnev, R. J. *Solid. State. Chem*. **1991**, *94*, 220.
19. Zhao, J.; Wang, X.; Liu, C.; Xu, X.; Li, Y. *Powder. Tech*. **2008**, *183*, 220.
20. Kim, S.-S.; Yum, H.-H.; Sung, Y.-E. *Sol. Energy. Mater. Sol. Cells* **2003**, *79*, 495.
21. Kubelka, P.; Munk, F. Z. *Tech. Phys*. **1931**, *12*, 593.
22. Subramanian, M. A.; Aravamudan, G.; Subbaa Rao, G. V. *Prog. Solid. State. Chem*. **1983**, *15*, 55.

23. Barton, D. G.; Shtein, M.; Wilson, R. D.; Soled, S. L.; Iglesia, E. *J. Phys. Chem*. *B* **1999**, *103*, 630.
24. Tauc, J. *Mater. Res. Bull*. **1970**, *5*, 721.
25. Karunakaran, C.; Anilkumar, P.; Manikandan, G.; Gomathisankar, P. *Sol. Energy. Mater. Sol. Cells* **2010**, *94*, 900.
26. Mizoguchi, H.; Eng, H. W.; Woodward, P. M. *Inorg. Chem*. **2004**, *43*, 1667.